Effect of Doppler broadening on Autler-Townes splitting in the molecular cascade excitation scheme

E. Ahmed and A. M. Lyyra
Department of Physics, Temple University, Philadelphia, Pennsylvania 19122, USA
(Received 10 July 2007; published 9 November 2007)

Theoretical analysis of the Autler-Townes splitting pattern in a three-level cascade excitation of a Doppler-broadened sample reveals that the observed Autler-Townes splitting is not only a function of the coupling-laser Rabi frequency, as in the homogeneously broadened case, but can also strongly depend on the wavenumber ratio of the coupling and probe lasers. Utilizing a steady-state density matrix formalism, we derive exact expressions for the populations of the intermediate and upper levels for a homogeneously broadened system. In the limit of a weak probe field, analytical expressions for Doppler-broadened excitation spectra from the intermediate and upper levels are derived. Using these expressions, we investigate the critical role of Doppler broadening on the observation of Autler-Townes splitting and its asymptotic behavior as a function of the coupling Rabi frequency for counterpropagating and copropagating configurations for different wavenumber ratios of the lasers.

DOI: 10.1103/PhysRevA.76.053407 PACS number(s): 33.40.+f, 42.50.Hz

INTRODUCTION

Recent strong interest in coherence and quantum interference effects such as the Autler-Townes (AT) effect [1] and electromagnetically induced transparency (EIT) [2,3] in atomic and molecular systems is due to novel applications such as measurement of the absolute value of the transition dipole moment [4,5], production of slow light [6], and manipulation of the index of refraction [7]. Very often in such experiments gas-phase atomic and molecular systems are used, in which the inhomogeneous Doppler line broadening is much larger than the homogeneous broadening.

There has been extensive theoretical and experimental work on three-level atomic and molecular systems. The general theoretical description of a three-level atom was given by [8,9]. For some of the different aspects and configurations of the three-level systems one can see [10–20] and the references therein. We would like to mention particularly the works by Salomaa and Stenholm on Doppler-free [21] and Doppler-broadened [22] cascade schemes in the limit of a weak probe laser with the coupling laser on resonance between the ground and intermediate states. For this arrangement, experimental results on the AT splitting in the context of transition dipole moment measurements between the ground $X\ ^1\Sigma_g^+$ and the excited $A\ ^1\Sigma_u^+$ states for Na_2 are given in [5].

In the presented work we consider the effect of inhomogeneous Doppler broadening on the observation of AT splitting in the excitation spectra of a cascade open molecular system given in Fig. 1. In contrast to the works [21,22] mentioned in the above paragraph, we consider a variant of the cascade scheme where the coupling laser is on resonance between the intermediate and upper levels. This cascade configuration has been employed experimentally in Refs. [4,23,24] for observation of EIT and AT splitting in alkali-metal dimers. The theoretical considerations presented in this paper are in close relation to these experimental works. For our calculations we use the well-known and widely used density matrix formalism [11,25]. Since the calculations are in relation to molecular systems, we have introduced two additional levels $|4\rangle$ and $|5\rangle$ as given in Fig. 1 to represent all possible extra levels to which decay from levels $|2\rangle$ and $|3\rangle$ is possible due to spontaneous emission. The two laser beams interacting with the system propagate along a common axis z either in copropagating or counterpropagating configuration. We assume that each laser is on resonance with only one transition. The first laser L_1 (the probe) couples the levels $|1\rangle$ and $|2\rangle$, while the second laser L_2 (the coupling) couples the levels $|2\rangle$ and $|3\rangle$.

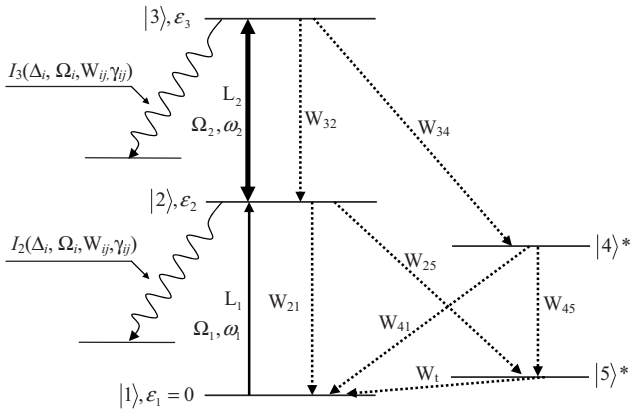

FIG. 1. Schematic diagram of excitation and decay processes of the three-level, double-resonance cascade scheme. The probe laser L_1 with optical frequency ω_1 and Rabi frequency Ω_1 is tuned through the resonance of levels $|1\rangle$ and $|2\rangle$, while the coupling laser L_2 with optical frequency ω_2 and Rabi frequency Ω_2 is on resonance with levels $|2\rangle$ and $|3\rangle$. Here $I_2(\Delta_i, \Omega_i, \gamma_{ij})$ and $I_3(\Delta_i, \Omega_i, \gamma_{ij})$ represent the intensities of the single-channel fluorescence usually used for detection in the experiments with molecules [4,23,24]; they are proportional to the populations of levels $|2\rangle$ and $|3\rangle$. The dashed arrows indicate possible decay channels from the different energy levels. Due to selection rules W_{31}, W_{24} and W_{35} are zero for homonuclear molecules. Levels $|4\rangle^*$ and $|5\rangle^*$ indicate other possible decay channels rendering the system open. The beam-transit rate W_t is added to account for the rate with which the molecules escape the interaction region. It is only significant for level $|5\rangle^*$ since it cannot radiatively decay, $W_{51}=W_t$.

HOMOGENEOUSLY BROADENED SYSTEM

The evolution of the density matrix $\rho(\mathbf{v},\mathbf{r},t)$ of our system in time and space is governed by the equation of motion

$$\frac{\partial\rho}{\partial t} = -\frac{i}{\hbar}[H_I,\rho] + \Gamma(\rho). \tag{1}$$

The Hamiltonian H_I in the interaction picture with the rotating wave approximation taken into account has the form

$$H_I = \hbar\Delta_1|2\rangle\langle 2| + \hbar(\Delta_1+\Delta_2)|3\rangle\langle 3| + \hbar\frac{\Omega_1}{2}(|2\rangle\langle 1| + |1\rangle\langle 2|) + \hbar\frac{\Omega_2}{2}(|3\rangle\langle 2| + |2\rangle\langle 3|), \tag{2}$$

where the detunings Δ_1 and Δ_2 are defined by $\Delta_1=\omega_{21}-\omega_1$ and $\Delta_2=\omega_{32}-\omega_2$, and ω_{21} and ω_{32} are the corresponding transition frequencies for the $|1\rangle\leftrightarrow|2\rangle$ and $|2\rangle\leftrightarrow|3\rangle$ transitions. The Hamiltonian in Eq. (2) does not involve levels $|4\rangle$ and $|5\rangle$ since they are not coherently coupled to any other levels. Every molecular level can decay to lower-lying states of the system through spontaneous emission, as well as other processes such as collisions, etc. They are incorporated in the density matrix equation of motion by means of an $n\times n$ relaxation matrix $\Gamma(\rho)$, with $n=5$ for the system depicted in Fig. 1. The elements of the matrix $\Gamma(\rho)$ in general can be represented in the form

$$\Gamma_{ij}(\rho) = \delta_{ij}\left(-W_i\rho_{ij} + \sum_{\substack{k=1\\k\neq i}}^{n}\Theta(\varepsilon_k-\varepsilon_i)W_{ki}\rho_{kk}\right) - (1-\delta_{ij})\gamma_{ij}\rho_{ij}, \tag{3}$$

where δ_{ij} is Kronecker's delta and $\Theta(\varepsilon_k-\varepsilon_i)$ is the Heaviside step function. ε_i denotes the energy of level $|i\rangle$. With W_{ij} we denote the radiative decay rate from level i to level j, W_i is the total radiative decay rate of level i, and γ_{ij} are phenomenological parameters representing the damping rate at which the off-diagonal elements of the density matrix relax toward equilibrium, defined by

$$\gamma_{nm} = \frac{1}{2}\sum_k (W_{nk}+W_{mk}) + \gamma_{nm}^c, \quad n\neq m. \tag{4}$$

The γ_{nm}^c parameters represent the dependence of the decay processes on collisions with other atoms or molecules.

Since the molecules are in motion, the presence of a velocity component along the propagation axis z of the laser beams, leads to a Doppler shift of the frequency of each laser as observed from the rest frame of the molecule. Thus, we define the velocity-dependent detuning of the laser frequencies of L_1 and L_2 from the molecular transitions as $\delta_1 \equiv \Delta_1 \pm k_1 v_z$ and $\delta_2 \equiv \Delta_2 + k_2 v_z$, respectively. Here k_1 and k_2 are the wavenumbers of the corresponding laser, v_z is the molecular velocity component along the laser propagation axis z, and the sign for $\pm k_1 v_z$ is chosen in accordance with the propagation direction of L_1, with respect to L_2.

Taking into account the molecular motion, the Hamiltonian H_I becomes

$$H_I = \hbar\delta_1|2\rangle\langle 2| + \hbar(\delta_1+\delta_2)|3\rangle\langle 3| + \hbar\frac{\Omega_1}{2}(|2\rangle\langle 1| + |1\rangle\langle 2|) + \hbar\frac{\Omega_2}{2}(|3\rangle\langle 2| + |2\rangle\langle 3|). \tag{5}$$

Since we only consider cw laser excitations, we have a steady state and $\dot{\rho}=0$, which reduces Eq. (1) from a system of differential equations of first order to a set of homogeneous linear equations. Because the total population in the system is conserved, we have the additional condition

$$1 = \rho_{11}+\rho_{22}+\rho_{33}+\rho_{44}+\rho_{55}. \tag{6}$$

Combining Eq. (5) with the equation of motion (1) and including all the possible decay processes depicted in Fig. 1 in $\Gamma(\rho)$, we obtain the individual components of the density matrix equation of motion:

$$0 = i\Omega_1(\rho_{12}-\rho_{21}) + 2W_2\rho_{22} + 2W_{34}\rho_{33}, \tag{7a}$$

$$0 = 2d_1\rho_{12} - i\Omega_1(\rho_{22}-\rho_{11}) + i\Omega_2\rho_{13}, \tag{7b}$$

$$0 = i\Omega_2\rho_{12} + 2d_2\rho_{13} - i\Omega_1\rho_{23}, \tag{7c}$$

$$0 = 2\tilde{d}_1\rho_{21} + i\Omega_1(\rho_{22}-\rho_{11}) - i\Omega_2\rho_{31}, \tag{7d}$$

$$0 = -i\Omega_1\rho_{13} + i\Omega_2(\rho_{22}-\rho_{33}) + 2d_3\rho_{23}, \tag{7e}$$

$$0 = -i\Omega_2\rho_{21} + 2\tilde{d}_2\rho_{31} + i\Omega_1\rho_{32}, \tag{7f}$$

$$0 = i\Omega_1\rho_{31} - i\Omega_2(\rho_{22}-\rho_{33}) + 2\tilde{d}_3\rho_{32}, \tag{7g}$$

$$0 = i\Omega_2(\rho_{23}-\rho_{32}) + 2W_3\rho_{33}, \tag{7h}$$

where we have eliminated the terms involving the levels $|4\rangle$ and $|5\rangle$. This is easily performed, since they are noncoherently coupled to the rest of the system. With d_1, d_2, and d_3 we denote the complex detunings, defined by $d_1=i\delta_1-\gamma_{12}$, $d_2=i\delta_1+i\delta_2-\gamma_{13}$, and $d_3=i\delta_2-\gamma_{23}$, and $\tilde{d}_i$ is the complex conjugate of d_i. In the system of linear equations (7) only the linearly independent components of Eq. (1) are included. The population conservation condition (6) with ρ_{44} and ρ_{55} eliminated has the form

$$1 = \rho_{11} + (a-1)\rho_{22} + b\rho_{33}. \tag{8}$$

The parameters a and b are defined as

$$a = 2 + \frac{W_{25}}{W_t}, \tag{9}$$

$$b = 1 + \frac{W_{34}}{W_4}\left(1 + \frac{W_{45}}{W_t}\right). \tag{10}$$

Since our analysis applies mainly to experiments in which the detected signal is spectrally resolved fluorescence of a single rovibronic transition (called hereinafter "single-channel fluorescence"), the calculations emphasize the diagonal matrix elements, which are proportional to the popula-

tions of the corresponding levels. In cases where the experiments are based on absorption measurements, the off-diagonal density matrix elements are of importance. Due to the relative weakness of absorption by any single molecular rovibronic transition, fluorescence detection is mainly used in experiments involving molecules, while absorption measurements are frequently used in experiments with atoms.

The system of linear equations (7) combined with the population conservation condition (8) can be solved explicitly for any of the density matrix elements ρ_{ij}. After lengthy algebraic manipulations one obtains the following expression for ρ_{22} and ρ_{33}:

$$\rho_{22} = \Omega_1^2 \frac{\Omega_2^2\{(W_{34} - 2\gamma_{13})\mathrm{Re}[L] - D\} - W_3\,\mathrm{Re}[\tilde{D}_2 L]}{2A\tilde{L}L - \mathrm{Re}[(S_1 D_1 + \Omega_1^2 S_2)\tilde{L}] - \Omega_1^2\Omega_2^2(a+b)D}, \tag{11}$$

$$\rho_{33} = -\Omega_1^2\Omega_2^2 \frac{(W_2 + 2\gamma_{13})\mathrm{Re}[L] + D}{2A\tilde{L}L - \mathrm{Re}[(S_1 D_1 + \Omega_1^2 S_2)\tilde{L}] - \Omega_1^2\Omega_2^2(a+b)D}, \tag{12}$$

where A, L, S_i, D_i, and D are defined by

$$L = 4d_1 d_2 d_3 + d_1\Omega_1^2 + d_3\Omega_2^2, \tag{13}$$

$$A = W_2 W_3 - 2\gamma_{13}(bW_2 - aW_{34}), \tag{14}$$

$$S_1 = (bW_2 - aW_{34})D_2 + \Omega_2^2(W_2 + W_{34}), \tag{15}$$

$$S_2 = W_3 a D_2 + \Omega_2^2(2\gamma_{13}(a+b) - W_3), \tag{16}$$

$$D_1 = 4d_1 d_2 + \Omega_2^2, \tag{17}$$

$$D_2 = 4d_2 d_3 + \Omega_1^2, \tag{18}$$

$$D = 2(d_1 d_2 - \tilde{d}_1\tilde{d}_2)(d_2 d_3 - \tilde{d}_2\tilde{d}_3). \tag{19}$$

It is important to note that the above expressions for ρ_{22} and ρ_{33} are exact in the framework of the steady-state density matrix formalism. Unlike the perturbatively derived expressions [4,21], they are valid for any combinations of Rabi frequencies Ω_1 and Ω_2. In cases where the populations of levels $|2\rangle$ and $|3\rangle$ have to be known exactly, expressions (11) and (12) can be used instead of a numerical solution of the system of equations (7).

DOPPLER-AVERAGED EXCITATION SPECTRA

In this section we derive expressions for the Doppler-averaged excitation spectra $I_2(\Delta_i, \Omega_i, \ldots)$ and $I_3(\Delta_i, \Omega_i, \ldots)$ from levels $|2\rangle$ and $|3\rangle$, respectively. In order to obtain $I_k(\Delta_i, \Omega_i, \ldots)$, we average the homogeneously broadened excitation spectra, given by the population ρ_{kk} of the corresponding level, over the velocity distribution $N(v_z)$ of the molecules. Thus,

$$I_k = \int_{-\infty}^{+\infty} \rho_{kk}(v_z) N(v_z) dv_z, \tag{20}$$

where v_z is the z component of the velocity of the molecules. For the velocity distribution $N(v_z)$, we use the Maxwell-Boltzmann distribution

$$N(v_z) = \frac{N_0}{u\sqrt{\pi}} \exp\left(-\frac{v_z^2}{u^2}\right). \tag{21}$$

Although the expressions for ρ_{22} and ρ_{33} given by Eqs. (11) and (12) are simple rational functions of v_z, analytical calculation of the integral in Eq. (20) is not possible. Integrals of the type $R(\xi)e^{-\xi^2}$ can be evaluated analytically (in terms of special functions) by decomposing the rational function into elementary fractions. In our case, however, the denominator of ρ_{kk} is a polynomial of sixth order with respect to v_z, with nonzero complex coefficients, making the decomposition practically impossible.

In order to overcome this difficulty, one has to resort to some form of simplification of Eqs. (11) and (12). The most straightforward and widespread approach is to consider the Rabi frequency of one of the lasers (probe) as a weak perturbation. Hereafter we assume that L_1 is the probe laser and L_2 is the coupling laser with the condition $\Omega_1 \ll \Omega_2$ always fulfilled. In order to highlight the terms that can be neglected in the limit of a weak probe laser in Eqs. (11) and (12), we rewrite them in the forms given below.

For ρ_{22} we have

$$\rho_{22} = \Omega_1^2 \frac{\mathrm{Re}[M_0\tilde{D}_1] + M_1\Omega_1^2}{P|D_1|^2 - Q\Omega_1^2}, \tag{22}$$

with the terms in the numerator given by

$$M_0 = \Omega_2^2(W_{34}\tilde{d}_3 - 2\gamma_{23}d_2) - 4W_3|d_3|^2 d_2, \tag{23}$$

$$M_1 = 8\gamma_{12}W_3\,\mathrm{Re}[d_2 d_3] + W_3(\Omega_1^2\gamma_{12} + \gamma_{23}\Omega_2^2) - (W_{34} - 2\gamma_{13})\gamma_{12}\Omega_2^2. \tag{24}$$

For ρ_{33} we have

$$\rho_{33} = \Omega_1^2\Omega_2^2 \frac{\mathrm{Re}[L_0\tilde{D}_1] + L_1\Omega_1^2}{P|D_1|^2 - Q\Omega_1^2}, \tag{25}$$

with the terms in the numerator given by

$$L_0 = -W_2\tilde{d}_3 - 2\gamma_{23}d_2, \tag{26}$$

$$L_1 = \gamma_{12}(W_2 + 2\gamma_{13}). \tag{27}$$

The quantities in the denominators of Eqs. (22) and (25) are defined by

$$P = 2W_2 W_3|d_3|^2 + \gamma_{23}(W_2 + W_{34})\Omega_2^2, \tag{28}$$

$$Q = \mathrm{Re}[(S_1\tilde{d}_1 + \tilde{S}_2 d_3 - 4A\tilde{d}_1 d_3)D_1 + \Omega_1^2 S_2 \tilde{d}_1] - \gamma_{23}(bW_2 - aW_{34})|D_1|^2 + \Omega_2^2(a+b)D - 2A|d_1|^2\Omega_1^2. \tag{29}$$

By keeping the leading term of Ω_1^2 and setting $\Omega_1 = 0$ everywhere else, we obtain

$$\rho_{22}^p = \Omega_1^2 \frac{\mathrm{Re}[M_0\tilde{D}_1]}{P|D_1|^2} = \frac{\Omega_1^2}{P}\,\mathrm{Re}\left[\frac{M_0}{D_1}\right], \tag{30}$$

$$\rho_{33}^p = \Omega_1^2\Omega_2^2 \frac{\mathrm{Re}[L_0\tilde{D}_1]}{P|D_1|^2} = \frac{\Omega_1^2\Omega_2^2}{P}\,\mathrm{Re}\left[\frac{L_0}{D_1}\right]. \tag{31}$$

Expressions (30) and (31) are exactly the same as in [4], where they are derived from the system of equations similar to Eqs. (7) by applying perturbative theory in Ω_1 directly to the system of linear equations. We note also that Eq. (31) is similar to the expression for ρ_{33}^p given in [21] for a cascade scheme where the coupling laser acts on the transition $|1\rangle$-$|2\rangle$ while the probe acts on the $|2\rangle$-$|3\rangle$ transition. The denominators of the above ρ_{22}^p and ρ_{33}^p expressions are a product of two parts P and D_1, each being a polynomial of second order in v_z. Thus, the decomposition into elementary fractions can be done without any difficulties.

To make all further considerations simpler and more transparent, we use the dimensionless variables

$$z = \frac{v_z}{u}, \quad \Omega_i' = \frac{\Omega_i}{k_2 u}, \quad \gamma_{ij}' = \frac{\gamma_{ij}}{k_2 u}, \quad W_i' = \frac{W_i}{k_2 u}, \quad \Delta_i' = \frac{\Delta_i}{k_2 u} \tag{32}$$

In addition, we omit the primes for simplicity unless noted otherwise. Next, we write ρ_{kk}^p in the form

$$\rho_{22}^p = \frac{C_2}{(z+\Delta_2)^2 + W^2}\,\mathrm{Im}\left[\frac{a_0 + a_1 z + a_2 z^2 + a_3 z^3}{(z-z_1)(z-z_2)}\right], \tag{33}$$

$$\rho_{33}^p = \frac{C_3}{(z+\Delta_2)^2 + W^2}\,\mathrm{Im}\left[\frac{b_0 + b_1 z}{(z-z_1)(z-z_2)}\right], \tag{34}$$

with W, B, z_1, z_2, a_0, a_1, a_2, a_3, b_0, and b_1 defined by

$$W^2 = \gamma_{23}^2 + \frac{\gamma_{23}(W_2 + W_{34})\Omega_2^2}{2W_2W_3}, \tag{35}$$

$$C_2 = -\frac{\Omega_1^2}{8x(1+x)W_2W_3}, \quad C_3 = -\Omega_2^2 C_2 \tag{36}$$

$$z_{1,2} = -\frac{1}{2}\left(\frac{e_1}{x} + \frac{e_2}{(1+x)}\right) \pm \frac{1}{2}\sqrt{\left(\frac{e_1}{x} - \frac{e_2}{(1+x)}\right)^2 + \frac{\Omega_2^2}{x(1+x)}}, \tag{37}$$

$$a_0 = \Omega_2^2(W_{34}\tilde{e}_3 + 2\gamma_{23}e_2) + 4W_3 e_2|e_3|^2, \tag{38}$$

$$a_1 = \Omega_2^2[W_{34} + 2\gamma_{23}(1+x)] + 4W_3[|e_3|^2(1+x) + (e_3 + \tilde{e}_3)e_2], \tag{39}$$

$$a_2 = 4W_3[e_2 + (e_3 + \tilde{e}_3)(1+x)], \tag{40}$$

$$a_3 = 4W_3(1+x), \tag{41}$$

$$b_0 = W_2\tilde{e}_3 - 2\gamma_{23}e_2, \tag{42}$$

$$b_1 = W_2 - 2\gamma_{23}(1+x), \tag{43}$$

where $e_1 = \Delta_1 + i\gamma_{12}$, $e_2 = \Delta_1 + \Delta_2 + i\gamma_{13}$, $e_3 = \Delta_2 + i\gamma_{23}$, and x is the ratio of the probe and coupling laser wavenumbers k_1 and k_2, respectively. In order to simultaneously treat copropagating and counterpropagating beam configurations, x carries a sign. We define

$$x = \frac{k_1}{k_2}, \quad x < 0 \quad \text{for counterpropagating laser beams,}$$
$$x > 0 \quad \text{for copropagating laser beams.} \tag{44}$$

We proceed by expanding Eqs. (33) and (34) into partial fractions

$$\rho_{22}^p = \sum_{k=1}^{2} \mathrm{Im}\left[A_k\left(\frac{1}{z-z_k} - \frac{z_k + 2\Delta_2 + z}{(z+\Delta_2)^2 + W^2}\right)\right] + \frac{\gamma_{12}\Omega_1^2}{2W_2x^2}\frac{1}{(z+\Delta_2)^2 + W^2}, \tag{45}$$

$$\rho_{33}^p = \sum_{k=1}^{2} \mathrm{Im}\left[B_k\left(\frac{1}{z-z_k} - \frac{z_k + 2\Delta_2 + z}{(z+\Delta_2)^2 + W^2}\right)\right]. \tag{46}$$

The coefficients A_k and B_k are given by

$$A_k = (-1)^{k-1}C_2\frac{a_0 + a_1 z_k + a_2 z_k^2 + a_3 z_k^3}{(z_k+\Delta_2)^2 + W^2}\frac{1}{z_1 - z_2} \quad \text{for } k = 1,2, \tag{47}$$

$$B_k = (-1)^{k-1}C_3\frac{b_0 + b_1 z_k}{(z_k+\Delta_2)^2 + W^2}\frac{1}{z_1 - z_2} \quad \text{for } k = 1,2. \tag{48}$$

Combining Eqs. (45) and (46) with Eq. (20), we obtain

$$I_2 = \sum_{k=1}^{2} \mathrm{Im}\left[A_k\int_{-\infty}^{+\infty}\frac{e^{-z^2}}{z-z_k}dz - A_k\int_{-\infty}^{+\infty}\frac{z_k + 2\Delta_2 + z}{(z+\Delta_2)^2 + W^2}e^{-z^2}dz\right] + \frac{\gamma_{12}\Omega_1^2}{2W_2x^2}\int_{-\infty}^{+\infty}\frac{e^{-z^2}}{(z+\Delta_2)^2 + W^2}dz, \tag{49}$$

$$I_3 = \sum_{k=1}^{2} \mathrm{Im}\left[B_k\int_{-\infty}^{+\infty}\frac{e^{-z^2}}{z-z_k}dz - B_k\int_{-\infty}^{+\infty}\frac{z_k + 2\Delta_2 + z}{(z+\Delta_2)^2 + W^2}e^{-z^2}dz\right], \tag{50}$$

where we have omitted the factor $N_0/\sqrt{\pi}$ for simplicity. The integrals in Eqs. (49) and (50) can be expressed in terms of the Faddeeva function $w(z) = e^{-z^2}\mathrm{erfc}(-iz)$ [26,27]. This yields

$$I_2 = \pi \sum_{k=1}^{2} \mathrm{Re}[A_k\{w(z_k) - 2\Theta(\mathrm{Re}[iz_k])e^{-z_k^2}\}] + \pi \sum_{k=1}^{2} \mathrm{Im}\left[A_k \,\mathrm{Im}[w(-\Delta_2 + iW)] - \frac{A_k(z_k + \Delta_2)}{W} \mathrm{Re}[w(-\Delta_2 + iW)]\right] + \frac{\gamma_{12}\Omega_1^2}{2W_2 x^2}\frac{\pi}{W} \mathrm{Re}[w(-\Delta_2 + iW)], \quad (51)$$

$$I_3 = \pi \sum_{k=1}^{2} \mathrm{Re}[B_k\{w(z_k) - 2\Theta(\mathrm{Re}[iz_k])e^{-z_k^2}\}] + \pi \sum_{k=1}^{2} \mathrm{Im}\left[B_k \,\mathrm{Im}[w(-\Delta_2 + iW)] - B_k \frac{(z_k + \Delta_2)}{W} \mathrm{Re}[w(-\Delta_2 + iW)]\right], \quad (52)$$

where $\Theta(\zeta)$ is the Heaviside step function. Thus, in the framework of the perturbative population densities ρ_{kk}^p we obtain analytical expressions for the Doppler-broadened excitation spectra of the intermediate and upper levels for the cascade excitation scheme given in Fig. 1.

In most experiments the coupling field is kept on or very close to resonance. For this reason and in order to simplify the analysis that follows algebraically, we set the detuning of the coupling laser to zero ($\Delta_2 = 0$). Thus, we obtain

$$I_2 = \pi \sum_{k=1}^{2} \mathrm{Re}[A_k\{w(z_k) - 2\Theta(\mathrm{Re}[iz_k])e^{-z_k^2}\}] + \pi A e^{W^2} \mathrm{erfc}(W), \quad (53)$$

$$I_3 = \pi \sum_{k=1}^{2} \mathrm{Re}[B_k\{w(z_k) - 2\Theta(\mathrm{Re}[iz_k])e^{-z_k^2}\}] + \pi B e^{W^2} \mathrm{erfc}(W), \quad (54)$$

$$A = \frac{\gamma_{12}\Omega_1^2}{2W_2 W x^2} - \frac{1}{W} \sum_{k=1}^{2} \mathrm{Im}[A_k z_k], \quad (55)$$

$$B = -\frac{1}{W} \sum_{k=1}^{2} \mathrm{Im}[B_k z_k], \quad (56)$$

where we used the relation $w(iy) = e^{y^2}\mathrm{erfc}(y)$, for y real.

Note that I_2 and I_3 consist of two distinct dominant parts

$$\mathrm{Re}[A_k\{w(z_k) - 2\Theta(\mathrm{Re}[iz_k])e^{-z_k^2}\}], \quad \text{for } I_2 \quad (k = 1,2), \quad (57)$$

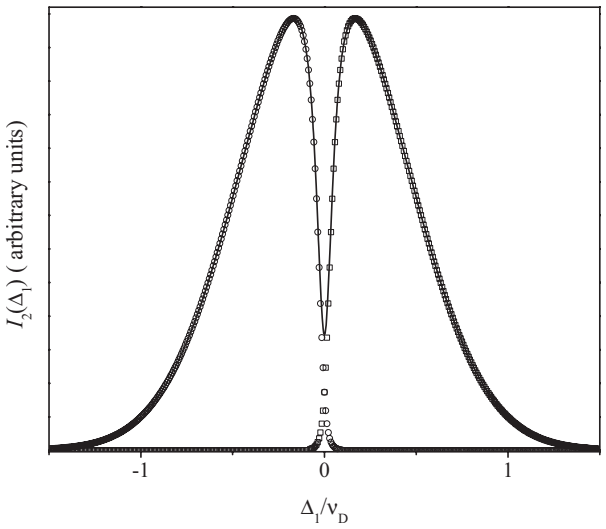

FIG. 2. The solid black line corresponds to $I_2(\Delta_1)$ as calculated from Eq. (53), the plot with the open circles shows Eq. (57) for $k=1$, and the plot with the open squares shows Eq. (57) for $k=2$, for $x=-1.2$, and $\Omega_2 = 100$ MHz.

$$\mathrm{Re}[B_k\{w(z_k) - 2\Theta(\mathrm{Re}[iz_k])e^{-z_k^2}\}], \quad \text{for } I_3 \quad (k = 1,2). \quad (58)$$

For each I_i the two terms for $k=1$ and $k=2$ added together form the basic shape of the spectra. The term proportional to $e^{W^2}\mathrm{erfc}(W)$ is usually negligible. The presence or the absence of the AT splitting and EIT features, and others depends on the degree of overlap between these two dominant parts of I_2 and I_3, as shown in Figs. 2 and 3. In the calculations for these figures the parameters we have used are for the Na_2 dimer system with level $|2\rangle$ corresponding to a rovibrational level of the $A\ ^1\Sigma_u^+$ state with a lifetime of $\tau_2 = 12.5$ ns [28] and with level $|3\rangle$ corresponding to a rovibrational level of a higher

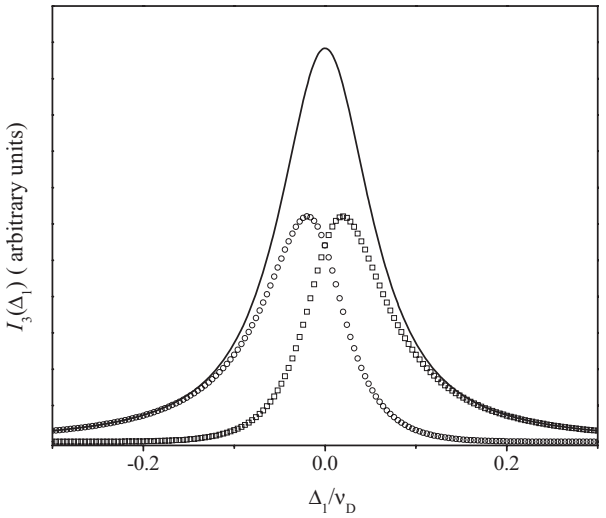

FIG. 3. The solid black line corresponds to $I_3(\Delta_1)$ calculated from Eq. (54), the plot with the open circles shows Eq. (58) for $k=1$, and the plot with the open squares shows Eq. (58) for $k=2$, for $x=-1.2$, and $\Omega_2 = 100$ MHz.

excited state, in our case $2\ ^1\Pi_g$, with lifetime of $\tau_3=18$ ns [5] and branching ratio $W_{32}=0.1W_3$. The Doppler linewidth is $\nu_D=1.1$ GHz corresponding approximately to a temperature of 550 K and transition wavenumber of 15 000 cm^{-1} for the $|2\rangle$-$|1\rangle$ transition. No collisional dephasing rates are included, and no magnetic sublevel structure of the rovibrational levels is taken into account. In all further calculations and plots, we will use this set of parameters, unless stated otherwise.

AUTLER-TOWNES SPLITTING IN THE FLUORESCENCE EXCITATION SPECTRA

Although the AT splitting for the scheme we are considering is present in the intermediate and upper levels, experimentally in Doppler-broadened molecular systems it is very difficult to be observed from the intermediate state due to the inhomogeneous Doppler broadening. Instead, from the intermediate level one can observe on the background of the Doppler-broadened excitation spectra the narrow EIT feature as shown by [4,23,24]. Thus, the AT splitting in the cascade scheme we are considering is mainly observed from the upper level $|3\rangle$, when the coupling laser is fixed on resonance and the probe laser is scanned. For this reason in the analysis that follows we will work with the excitation spectra $I_3(\Delta_2=0)$ given by Eq. (54).

As shown by the experimental results given in Refs. [24,29], the AT splitting in the excitation spectra of level $|3\rangle$ in a Doppler-broadened sample is strongly dependent on the wavenumber ratio $|x|=k_1/k_2$ of the two lasers. For counterpropagating laser beams ($x<0$) the experimental results show a distinct difference between the case $-1<x<0$, where the wavenumber of the probe laser k_1 is smaller than the wavenumber of the coupling laser k_2, and the case $x<-1$, where k_1 is larger than k_2. In the case $-1<x<0$ [4,29] the AT splitting in $|3\rangle$ can be observed even at fairly small coupling Rabi frequencies. In contrast, when $x<-1$ the experimental fluorescence spectra [24,29] show that the AT splitting cannot be observed in the range of the experimentally accessible coupling laser Rabi frequencies of up to 500 MHz. In the latter case, even though the AT splitting is not observed from level $|3\rangle$, the spectrum from the intermediate level $|2\rangle$ clearly shows the EIT effect, thus indicating the presence of the AT effect in the system. In addition, simulations with only homogeneous broadening present show the AT splitting in both cases. This indicates that the appearance of the AT splitting in an inhomogeneously Doppler-broadened system is governed by the averaging over the velocity distribution of the molecules. As shown in Fig. 4, there are two types of features in the spectra of level $|3\rangle$: one narrow and sharp, dominant at smaller Rabi frequencies, and a broad one appearing in the spectra at very large Ω_2. The analysis of the expression for $I_3(\Delta_1)$ in Eq. (54) shows that the sharp narrow feature is due to the term $1/(z_1-z_2)$ present in the coefficients B_k, while the broad feature is due to the $w(z_k)$ terms.

From the condition $\frac{dI_3}{d\Delta_1}=0$ for an extremum of $I_3(\Delta_1)$ with respect to Δ_1, we can calculate the AT splitting as a function of the Rabi frequency of the coupling laser Ω_2. Results for such calculations are shown in Fig. 5 for three different values of x. The curve with $x=-0.9$ (i.e., $k_1<k_2$) is an example for the case of counterpropagating probe and coupling lasers. The case $x=-1.2$ also is an example of a counterpropagating configuration, but with $k_1>k_2$ and the curve with $x=0.9$ represents a copropagating configuration. As the Doppler linewidth is kept the same in all three cases (at $\nu_D=1.1$ GHz), changing the absolute value of x effectively corresponds to changing the value of k_2.

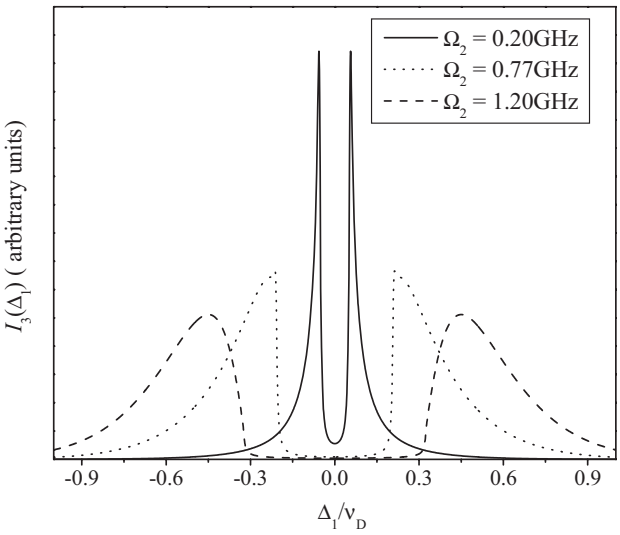

FIG. 4. Sample simulated spectra for level $|3\rangle$ for the Na_2 system described above with $x=-0.9$. The spectra represented by solid, dotted, and dashed lines correspond to coupling Rabi frequencies Ω_2 0.20, 0.77, and 1.20 GHz, respectively.

Figure 5 shows that AT splitting depends on Ω_2 in two ways. The first dependence appears at small Rabi frequencies, and only in the case of $-1<x<0$, is given by the term $1/(z_1-z_2)$. As discussed above, this corresponds to the sharp narrow features in Fig. 4. The second type of dependence exists for any value of x, but only at large enough values of

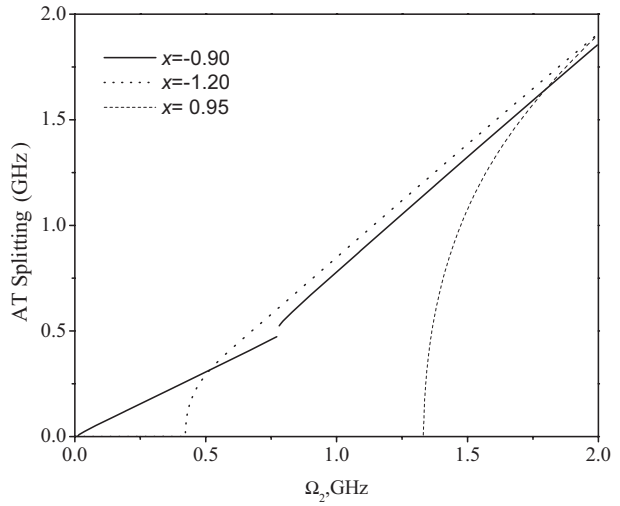

FIG. 5. The Autler-Townes splitting as a function of the Rabi frequency of the coupling laser Ω_2 for the Na_2 system for three different values of the ratio x.

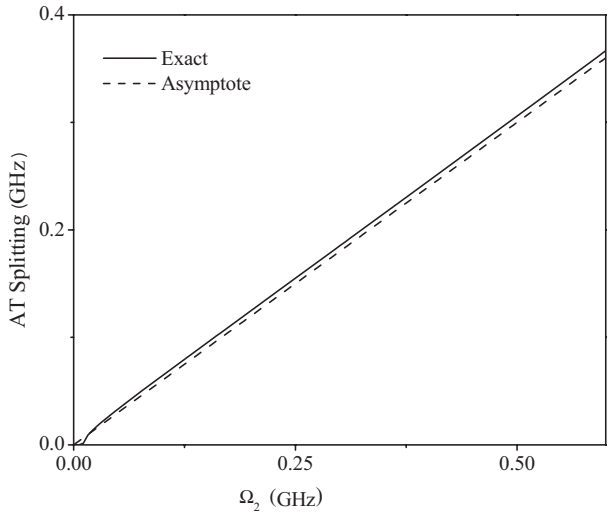

FIG. 6. Comparison between exact calculations (solid line) for the Autler-Townes splitting as a function of the coupling Rabi frequency Ω_2 and the asymptotic behavior (dashed line) given by Eq. (61) for $x=-0.9$.

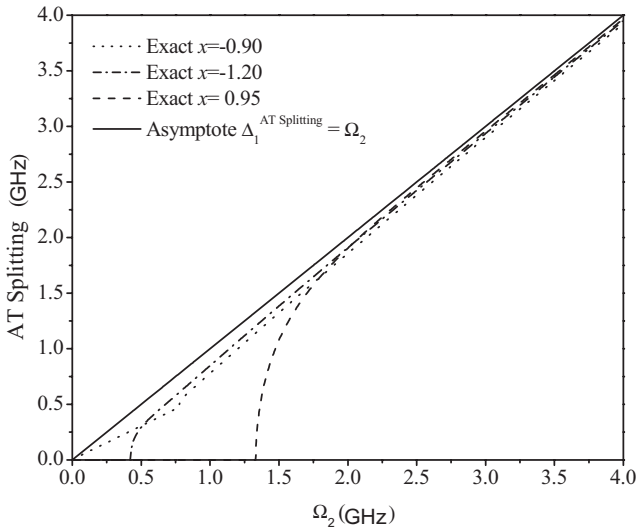

FIG. 7. Comparison between exact calculations for $x=-0.9$, -1.2, and 0.95 for Autler-Townes splitting as a function of the coupling Rabi frequency Ω_2 and the asymptotic behavior (solid line) given by Eq. (63).

Ω_2, and is given by the terms $w(z_k)$. The splitting due to the term $1/(z_1-z_2)$ has asymptotic linear behavior as in the case of the homogeneously broadened media, but the slope is different from unity and is, in general, a function of the ratio x. In order to understand why this is the case and why this type of splitting is only present for $-1<x<0$, we rewrite $1/(z_1-z_2)$ as

$$\frac{1}{z_1-z_2} = x(x+1)\sqrt{\frac{(\Delta_1-i\Gamma)^2+x(x+1)\Omega_2^2}{[\Delta_1^2-\Gamma^2+x(x+1)\Omega_2^2]^2+4\Gamma^2\Delta_1^2}}, \tag{59}$$

with $\Gamma=\gamma_{12}(1+x)-x\gamma_{13}$.

The term under the square root,

$$\frac{1}{[\Delta_1^2-\Gamma^2+x(x+1)\Omega_2^2]^2+4\Gamma^2\Delta_1^2}, \tag{60}$$

resembles a Lorentzian function with respect to Δ_1^2. Using the resonance condition $\Delta_1^2-\Gamma^2+x(x+1)\Omega_2^2=0$ and the fact that Γ is usually a small parameter, we see that

$$\Delta_1^{AT\ splitting} = 2\sqrt{-x(1+x)}\Omega_2, \quad \text{for } -1<x<0, \tag{61}$$

where $\Delta_1^{AT\ splitting}$ is the peak-to-peak separation of the AT split spectra. In Fig. 6, the asymptotic behavior given by Eq. (61) is compared with exact calculations for the AT splitting. It is obvious that there is good agreement at large enough coupling Rabi frequencies, especially in the value of the slope, which is an important parameter in the determination of the transition dipole moment of the coupling transition [4]. The resonance condition in (60) exists only for $-1<x<0$, because the term $x(1+x)$ is negative. In contrast, when $x>0$ or $x<-1$, the term $x(1+x)$ is positive and the function (60) has an extremum as a function of Δ_1 only at $\Delta_1=0$. This unusual behavior of $1/(z_1-z_2)$ is the reason the AT splitting is only observed in the case of a counterpropagating laser configuration when $k_2>k_1$.

At large enough coupling Rabi frequencies, the $w(z_i)$ terms become dominant and determines the AT splitting and the shape of the spectra. If the argument of $w(z_i)$ satisfies $|z_i|\gg 1$ (always fulfilled for $\Omega_2\gg 1$), we have the asymptotic behavior $w(z_i)\sim \frac{i}{\sqrt{\pi}}\frac{1}{z_i}$ [27,30]. It can be easily shown that for large Ω_2 ($\gamma_{ij}\ll\Omega_2$) and correspondingly large AT splitting ($\gamma_{ij}\ll\Delta_1$) the denominator $z_i\tilde{z}_i$ of the asymptote has a minimum as a function of Δ_1 approximately when

$$\Delta_1(1+2x)\pm\sqrt{\Delta_1^2+x(1+x)\Omega_2^2}=0, \tag{62}$$

which gives us $\Delta_1=\pm\frac{\Omega_2}{2}$. Then, for the splitting $\Delta_1^{AT\ splitting}$ defined as the peak-to-peak separation, we have

$$\Delta_1^{AT\ splitting}=\Omega_2. \tag{63}$$

Expression (63) is identical with the case of only homogeneous broadening present in the system. As is obvious from Eq. (63), in this case the splitting does not depend on x. The AT splitting for any value of x and large enough Ω_2 reaches this asymptotic behavior (see Fig. 7).

As can be seen from Figs. 6 and 7, there is a minimum value of Ω_2 that is required in order for AT splitting to be observed. We denote this threshold value of the coupling laser Rabi frequency by Ω_2^T. It is obvious that Ω_2^T is strongly dependent on the ratio x. Since for the value of Ω_2 at which the splitting becomes experimentally observable $I_3(\Delta_1)$ has an inflection point at zero detuning, the condition

$$\left.\frac{d^2I_3(\Delta_1)}{d\Delta_1^2}\right|_{\Delta_1=0}=0 \tag{64}$$

may be used to calculate Ω_2^T. Results obtained using Eq. (64) as a function of the ratio x are given in Fig. 8. As the graph shows, Ω_2^T is very small in the counterpropagating case for

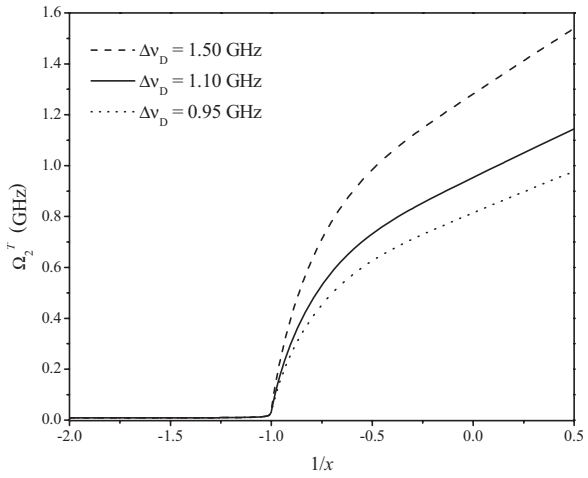

FIG. 8. Threshold Rabi frequency Ω_2^T as a function of $1/x$ for a set of Doppler linewidths of $\Delta\nu_D$=0.95, 1.10, and 1.50 GHz for the Na_2 system with k_1=15 000 cm^{-1}. These values of ν_D correspond to temperatures of 400 K, 550 K, and 1000 K.

$-1<x<0$ $(-\infty<1/x<-1)$ and does not depend on the Doppler linewidth. In the counterpropagating case with $x<-1$ $(-1<1/x<0)$ and for the copropagating case $x>0$ $(0<1/x<\infty)$, the Ω_2^T grows very rapidly with increasing $1/x$. Interpreted in experimental terms, the graph shows that the Autler-Townes splitting for a cascade scheme (Fig. 1) can be observed relatively easily in Doppler-broadened samples only for counterpropagating laser beams when the probe laser wavenumber k_1 is smaller than the coupling laser wavenumber k_2. In the case of copropagating laser beams, for any values of the wavenumbers k_1 and k_2, and in the case of counterpropagating beams, when the wavenumber of the probe laser k_1 is larger than the wavenumber of the coupling laser k_2, the splitting is very difficult to observe.

AUTLER-TOWNES SPLITTING ASYMPTOTE FOR EXPERIMENTAL MOLECULAR SYSTEMS

In real molecular systems [4,24] the experimentally recorded spectrum is a superposition of spectra originating between (with the selection rules taken into account) the different magnetic sublevels of the corresponding rovibrational levels. The Rabi frequency $\Omega_{i,M}$ between the corresponding sublevels is M dependent due to the M dependence of the transition dipole moment. Thus, expressions (61) and (63) can be interpreted only as the splitting asymptotes of a molecular system with given sublevel M. Since it is experimentally difficult to selectively couple specific M components [31], generalizing the AT splitting asymptotes to take into account the M sublevel structure of the molecular systems would be very useful. Keeping in mind that $C_3 \propto \Omega_1^2\Omega_2^2$ for the relative intensity of each M component we have

$$I_3^M(\Delta_1,\Omega_{1,M},\Omega_{2,M}) \propto \Omega_{1,M}^2\Omega_{1,M}^2. \tag{65}$$

Thus, if we find the maximum of this function with respect to M, we will have the effective M value, denoted by M^*, to determine the positions of the AT peaks in the resulting spectrum. M^* can be found from the condition

$$\frac{d\Omega_{1,M}^2\Omega_{1,M}^2}{dM} = 0 \tag{66}$$

for an extremum of the function $\Omega_{1,M}^2\Omega_{1,M}^2$. Next using the definition of Rabi frequency, Eq. (66) can be rewritten in terms of the transition dipole moments $\mu_{1,M}$ and $\mu_{2,M}$ as

$$\frac{d\mu_{1,M}^2\mu_{2,M}^2}{dM} = 0. \tag{67}$$

For example, for $^1\Sigma \rightarrow {}^1\Sigma$ and $^1\Sigma \rightarrow {}^1\Pi$ electronic transitions the M-dependent transition dipole moment $\mu_{i,M}$ between specific magnetic sublevels of $|i\rangle$ and $|i+1\rangle$ can be expressed as [32]

$$\mu_{i,M} = \mu_i^{\parallel} F_{^1\Sigma\rightarrow{}^1\Sigma}(J_i,J_{i+1},M) \quad \text{for } {}^1\Sigma \rightarrow {}^1\Sigma \text{ electronic transition}, \tag{68a}$$

$$\mu_{i,M} = \mu_i^{\perp} F_{^1\Sigma\rightarrow{}^1\Pi}(J_i,J_{i+1},M) \quad \text{for } {}^1\Sigma \rightarrow {}^1\Pi \text{ electronic transition}, \tag{68b}$$

where $\mu_i^{\parallel}$ and $\mu_i^{\perp}$ are the parallel and perpendicular components of the transition dipole moment between the $|i\rangle$ and $|i+1\rangle$ rovibrational levels with respect to the internuclear axis. $F_{^1\Sigma\rightarrow{}^1\Sigma}$ and $F_{^1\Sigma\rightarrow{}^1\Pi}$ are orientation factors [33–35]. The dependence of the orientation factors from J_i, J_{i+1}, and M is governed by the type of transition, the polarization of the corresponding laser field, and the rotational branch of the transition. Knowing M^* explicitly from Eqs. (67) and (68) for the AT splitting of the experimental spectrum, we can write

$$\Delta_1^{AT\ splitting} = 2\sqrt{-x(1+x)}\Omega_{2,M^*} = 2\sqrt{-x(1+x)}F(J_i,J_{i+1},M=M^*)\Omega_2. \tag{69}$$

We have calculated M^* for few often encountered transition combinations in diatomic alkali-metal dimer molecules, with the results given in Table I. For example, in the case of Ref.

TABLE I. Effective M^* for a linearly polarized probe (L_1) and coupling (L_2) laser for a set of possible electronic transition combinations.

$\lvert 1\rangle$-$\lvert 2\rangle$ \ $\lvert 2\rangle$-$\lvert 3\rangle$	$^1\Sigma \rightarrow {}^1\Sigma(^1\Pi), R$	$^1\Sigma \rightarrow {}^1\Sigma(^1\Pi), P$	$^1\Sigma \rightarrow {}^1\Pi, Q$
$^1\Sigma \rightarrow {}^1\Sigma, R$	$(1/\sqrt{2})\sqrt{(J_1+1)^2+(J_2+1)^2}$	$(1/\sqrt{2})\sqrt{(J_1+1)^2+J_2^2}$	$(1/\sqrt{2})(J_1+1)$
$^1\Sigma \rightarrow {}^1\Sigma, P$	$(1/\sqrt{2})\sqrt{J_1^2+(J_2+1)^2}$	$(1/\sqrt{2})\sqrt{J_1^2+J_2^2}$	$(1/\sqrt{2})J_1$

[4], where energy levels with $X\,^1\Sigma_g^+(v_1=4,J_1=15)$ for $|1\rangle$, $A\,^1\Sigma_g^+(v_2=13,J_2=14)$ for $|2\rangle$, and $G\,^1\Pi_g(v_3=11,J_3=14)$ for $|3\rangle$ were used in the experiment, for the factor in Eq. (69) we have $F(J_2)=\frac{|M|}{\sqrt{J_2(J_2+1)}}\big|_{M=M^*}$. Taking into account that $M^*=\frac{1}{\sqrt{2}}J_1$ and that the wavenumbers of the transitions are $k_1=15\,642.636\ \mathrm{cm}^{-1}$ and $k_2=17\,053.954\ \mathrm{cm}^{-1}$ $(x=-0.92)$ for the slope we obtain

$$2\sqrt{-x(1+x)}F(J_2,J_3,M=M^*)$$
$$=2\sqrt{-x(1+x)}\frac{J_1}{\sqrt{2J_2(J_2+1)}}=0.40. \qquad (70)$$

The corresponding value in [4] is 0.42, obtained from fitting the experimentally measured AT-split spectra as a function of the coupling Rabi frequency. Being able to calculate the slope of Eq. (69) in the simple way described above is of advantage, since the slope is a very important parameter in extracting the transition dipole moment from the experimentally measured AT-split spectra.

CONCLUSION

Employing the density matrix formalism in the steady-state limit we give exact expressions for the populations of the intermediate and upper levels of the cascade excitation scheme of Fig. 1 for the homogeneously broadened case. With the aid of perturbatively derived expressions for the excitation spectra we have studied the properties of the AT effect with the inhomogeneous Doppler broadening included. We showed that the Doppler broadening profoundly influences the observation of the AT splitting with a strong dependence of the splitting on the wavenumber ratio of the probe and coupling laser and their relative propagation direction. Additionally, we have investigated the asymptotic behaviors of the AT-splitting as a function of the coupling Rabi frequency and demonstrated a simple way of calculating the slope of the asymptote when the magnetic sublevels are taken into account. By analyzing the dependence of the threshold Rabi frequency Ω_2^T from the wavenumber ratio x and the Doppler linewidth $\Delta\nu_D$, we have provided a map of the optimal conditions for observing AT splitting when Doppler broadening is present.

ACKNOWLEDGMENTS

This material is based upon work supported by the National Science Foundation under Grants Nos. PHY 0245311 and PHY 0555608. We gratefully acknowledge discussions with Professor L. M. Narducci, Professor E. Arimondo, Professor F. C. Spano, Dr. A. Lazoudis, Dr. T. Kirova, Professor J. Magnes, and Professor J. Qi.

[1] S. H. Autler and C. H. Townes, Phys. Rev. **100**, 703 (1955).
[2] S. E. Harris, J. E. Field, and A. Imamoglu, Phys. Rev. Lett. **64**, 1107 (1990).
[3] K.-J. Boller, A. Imamoglu, and S. E. Harris, Phys. Rev. Lett. **66**, 2593 (1991).
[4] J. Qi, F. C. Spano, T. Kirova, A. Lazoudis, J. Magnes, L. Li, L. M. Narducci, R. W. Field, and A. M. Lyyra, Phys. Rev. Lett. **88**, 173003 (2002).
[5] E. Ahmed, A. Hansson, P. Qi, T. Kirova, A. Lazoudis, S. Kotochigova, A. M. Lyyra, L. Li, J. Qi, and S. Magnier, J. Chem. Phys. **124**, 084308 (2006).
[6] L. V. Hau, S. E. Harris, Z. Dutton, and C. H. Behroozi, Nature (London) **397**, 594 (1999).
[7] M. O. Scully and M. Fleischhauer, Phys. Rev. Lett. **69**, 1360 (1992).
[8] M. S. Feld and A. Javan, Phys. Rev. **177**, 540 (1969).
[9] T. Hansch and P. Toschek, Z. Phys. **236**, 213 (1970).
[10] E. Arimondo, Prog. Opt. **35**, 257 (1996).
[11] S. Stenholm, *Foundations of Laser Spectroscopy* (Wiley Interscience, New York, 1984).
[12] B. J. Feldman and M. S. Feld, Phys. Rev. A **5**, 899 (1972).
[13] J. E. Bjorkholm and P. F. Liao, Phys. Rev. A **14**, 751 (1976).
[14] M. Sargent III, Phys. Rep., Phys. Lett. **43**, 223 (1978).
[15] A. Schenzele and R. G. Brewer, Phys. Rep., Phys. Lett. **43**, 455 (1978).
[16] O. Poulsen and N. I. Winstrup, Phys. Rev. Lett. **47**, 1522 (1981).
[17] G. Grynberg and B. Cagnac, Rep. Prog. Phys. **40**, 791 (1977).
[18] R. R. Moseley, S. Shepherd, D. J. Fulton, B. D. Sinclair, and M. H. Dunn, Phys. Rev. A **53**, 408 (1996).
[19] H. R. Gray and C. R. Stroud, Jr., Opt. Commun. **25**, 359 (1978).
[20] S. Papademetriou, M. F. VanLeeuwen, and C. R. Stroud, Jr., Phys. Rev. A **53**, 997 (1996).
[21] R. Salomaa and S. Stenholm, J. Phys. B **8**, 1795 (1975).
[22] R. Salomaa and S. Stenholm, J. Phys. B **9**, 1221 (1976).
[23] J. Magnes, Ph.D. thesis, Temple University, 2003.
[24] A. Lazoudis, Ph.D. thesis, Temple University, 2005.
[25] M. O. Scully and M. S. Zubairy, *Quantum Optics* (Cambridge University Press, Cambridge, England, 2002).
[26] V. N. Faddeeva and N. M. Terentev, *Tables of Values of the Function w(z) for Complex Argument* (Pergamon Press, New York, 1961).
[27] *Handbook of Mathematical Functions with Formulas, Graphs, and Mathematical Tables*, Natl. Bur. Stand. Appl. Math. Ser. No. 55, edited by M. Abramowitz and I. A. Stegun (U.S. GPO, Washington, DC, 1972).
[28] G. Baumgartner, H. Kornmeier, and W. Preuss, Chem. Phys. Lett. **107**, 13 (1984).
[29] A. Lazoudis, E. Ahmed, L. Li, T. Kirova, P. Qi, A. Hansson, J. Magnes, F. C. Spano, and A. M. Lyyra, e-print arXiv:quant-ph/0508110.
[30] J. A. C. Weideman, SIAM (Soc. Ind. Appl. Math.) J. Numer. Anal. **31**, 1497 (1994).

[31] J. Qi, G. Lazarov, X. Wang, L. Li, L. M. Narducci, A. M. Lyyra, and F. C. Spano, Phys. Rev. Lett. **83**, 288 (1999).
[32] H. W. Kroto, *Molecular Rotation Spectra* (Wiley, London, 1975).
[33] R. S. Mulliken, Phys. Rev. **30**, 138 (1927).
[34] R. N. Zare, *Angular Momentum: Understanding Spatial Aspects in Chemistry and Physics* (Wiley, New York, 1988).
[35] F. C. Spano, J. Chem. Phys. **114**, 276 (2001).